Appendix A

Claim 1 *Let (y_i, z_i) denote the location of the i^{th} viewer row, ℓ_p the pixel size, ℓ_e the horizontal distance between two consecutive angular positions within the seat, and τ the distance between the vertical barrier and the screen (see Table 1). The z-coordinate of the slanted barrier ζ_i is a linear function of z_i,*

$$\zeta_i = \frac{\ell_p}{\ell_p + \ell_e} \cdot z_i + \frac{-\ell_e \tau}{\ell_p + \ell_e}, \tag{6}$$

and the y-coordinate $\rho_{i,j}$ is a function of z_i and ${y_o}^j$, the y-coordinate of the j^{th} vertical slit

$$\rho_{i,j} = {y_o}^j + \frac{(c_1 \cdot z_i + c_2) \cdot (c_3 \cdot z_i + c_4 - {y_o}^j)}{z_i} \tag{7}$$

where $c_1 = \frac{\ell_p}{\ell_p + \ell_e}$, $c_2 = \frac{-\ell_e}{\ell_p + \ell_e} \cdot \tau$, $c_3 = \frac{\Delta_y}{\Delta_z}$, $c_4 = y_1 - \frac{\Delta_y}{\Delta_z} z_1$.

Proof: The geometric relationship in the barrier structure defines a pair of similar triangles (see Fig. 18a) from which the following equation can be derived

$$\frac{\ell_p}{\ell_e} = \frac{(\zeta_i + \tau)}{z_i - \zeta_i}. \tag{8}$$

A short rearrangement of the terms in Eq. (8) leads to ζ_i as given by Eq. (6).

Similarly, $\rho_{i,j}$ can be derived using the similar triangles of Fig. 18b

$$\frac{\rho_{i,j} - {y_o}^j}{{y_o}^j - y_i} = \frac{-\zeta_i}{z_i} \Rightarrow \rho_{i,j} = {y_o}^j + \frac{{y_o}^j - y_i}{z_i}(-\zeta_i). \tag{9}$$

We express y_i as a linear function of z_i,

$$y_i = \frac{\Delta_y}{\Delta_z} \cdot z_i + y_1 - \frac{\Delta_y}{\Delta_z} z_1, \tag{10}$$

and substitute in Eq. (9) the ζ_i, y_i values from Eqs. (6) and (10), resulting in the $\rho_{i,j}$ values of Eq. (7). ■

Appendix B

Claim 2 *Denote by α_i the angle of rays from the i^{th} viewer row (y_i, z_i) towards the top slit ${y_o}^{n_y}$. To prevent ray blocking the slit spacing g should satisfy*

$$g \geq [\frac{{y_o}^{n_y} - y_1}{z_1} - \frac{{y_o}^{n_y} - y_m}{z_m}] \cdot \frac{-\zeta_1 z_1}{z_1 - \zeta_1} \tag{11}$$

or equivalently

$$g \geq (\alpha_1 - \alpha_m) \cdot \frac{-\zeta_1 z_1}{z_1 - \zeta_1} \tag{12}$$

Proof: The proof refers to the sketch in Fig. 19. Let us denote by $(\rho_{1,j-1}, \zeta_1)$ the intersection point of the ray from the first row with the slanted barrier at slit ${y_o}^{j-1}$, by $(\rho_{m,j}, \zeta_m)$ the intersection of the ray from the last row with the slanted barrier at slit ${y_o}^j$, and by $(\rho'_{m,j}, \zeta_1)$ the intersection of the same ray with the plane at depth ζ_1. To prevent the barriers from blocking rays, the following relation must hold

$$\rho_{1,j-1} \leq \rho'_{m,j}. \tag{13}$$

We can write the relationships between the y and z coordinates of the slanted horizontal parallax barrier and the viewers by looking at the similar triangles of Fig. 19.

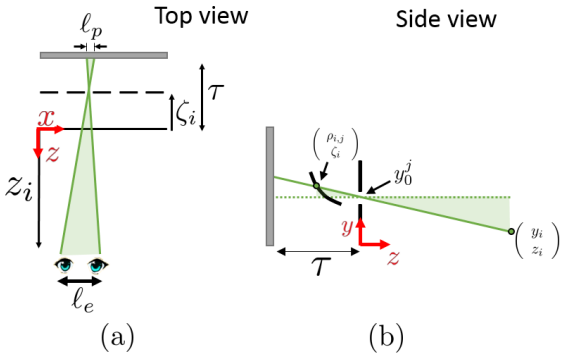

Figure 18: *Shaping the slanted barrier. To derive the x, y coordinates of the slanted barrier, i.e. ρ and ζ, we are looking at similar triangles in the geometry.*

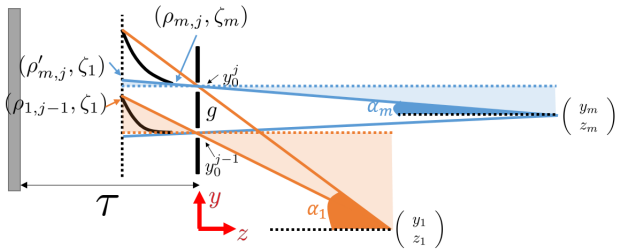

Figure 19: *Calculating the minimal slit separation. To prevent the slanted barriers from blocking each other, we force $\rho'_{m,j} \geq \rho_{1,j-1}$ (rays can cross each other after passing ζ_1).*

From the blue triangles:

$$\frac{\rho'_{m,j} - {y_o}^j}{{y_o}^j - y_m} = \frac{-\zeta_1}{z_m} \Rightarrow \rho'_{m,j} = {y_o}^j + \frac{-\zeta_1}{z_m}({y_o}^j - y_m). \tag{14}$$

From the orange triangles:

$$\frac{\rho_{1,j-1} - {y_o}^j}{{y_o}^{j-1} - y_1} = \frac{-\zeta_1}{z_1} \Rightarrow \rho_{1,j-1} = {y_o}^{j-1} + \frac{-\zeta_1}{z_1}({y_o}^{j-1} - y_1). \tag{15}$$

We can substitute ${y_o}^{j-1}$ in Eq. (15) by ${y_o}^j - g$ leading to

$$\rho_{1,j-1} = {y_o}^j - g + \frac{-\zeta_1}{z_1}({y_o}^j - g - y_1). \tag{16}$$

Substituting Eqs. (14) and (16) in Eq. (13) we get

$$g + \frac{-\zeta_1}{z_m}({y_o}^j - y_m) + \frac{\zeta_1}{z_1}({y_o}^j - g - y_1) \geq 0. \tag{17}$$

Rearranging Eq. (17) provides a lower bound on g

$$g \geq [\frac{{y_o}^j - y_1}{z_1} - \frac{{y_o}^j - y_m}{z_m}] \cdot \frac{-\zeta_1 z_1}{z_1 - \zeta_1}. \tag{18}$$

The highest value of the right-hand side of Eq. (18) is obtained at the top screen row, at $j = n_y$, leading to the g bound in Eq. (11).

Using first order approximation $(\tan\alpha \approx \alpha)$ on the geometric relationship of Fig. 19 we can write

$$\frac{{y_o}^{n_y} - y_1}{z_1} \approx \alpha_1, \qquad \frac{{y_o}^{n_y} - y_m}{z_1} \approx \alpha_m, \tag{19}$$

leading to Eq. (12). ■

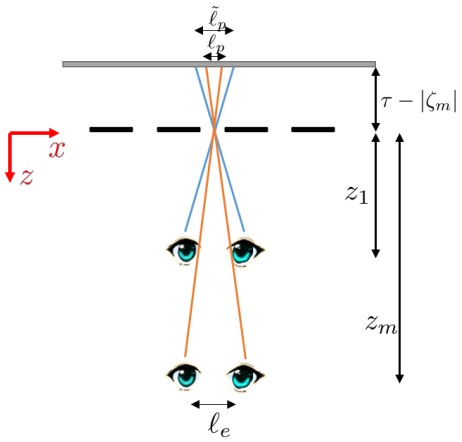

Figure 20: *A top view of the pinhole solution. The distance between the barrier and the screen was set to allow the last row to see pixels whose size is not lower than the native pixel size ℓ_p. A viewer at a closer row, however, sees wider pixels whose width $\tilde{\ell_p}$ was derived in the text. Thus the pinhole solution suffers from a horizontal resolution loss factor of $\tilde{\ell_p}/\ell_p$.*

Appendix C

In this section, we will analyze the resolution limits of the naive pinhole solution, and show that our proposed display has superior resolution in both the horizontal and vertical directions.

Horizontal resolution

As discussed in Sec. 2.3.2, the number of pixels our display supports horizontally is k times lower than the number of pixels on the screen, where k is the number of angular images. That is, if the native screen width supports N_x pixels, our angular images can include $n_x = N_x/k$ pixels.

To determine the resolution of the pinhole solution, note first that the minimal distance between the pinhole plane and the screen should be set such that the farthest row, which is the one obtaining the smallest disparity, can observe pixels whose size does not fall below ℓ_p (otherwise we have to under-sample the k angular images displayed for that row). However, closer rows achieve wider disparities and hence require wider pixels (see Figs. 10 and 20), and hence the resolution decreases. For example, in the cinema parameters considered at the beginning of Sec. 5, the resolution of the pinhole display is 1.7 times lower than in our display. The following claim derives the exact resolution gain.

Claim 3 *The x-axis resolution of our proposed display is $\frac{z_m}{z_1}$ times better than the x-axis resolution of the naive pinhole solution.*

Proof: Let N_x denote the number of horizontal pixels on the screen, and ℓ_p the native pixel size. The number of horizontal pixels in our proposed display is $n_x = N_x/k$, as discussed in Sec. 2.3.2.
Note that for any position of the pinhole array, geometry implies that the farthest row always achieves the smallest disparity on the screen. If our screen has pixels of size ℓ_p, and we do not want to under-sample the k different angular images that we display for that row, we can conclude from a similar triangle argument that the minimal distance between the pinhole plane and the screen must be

$$(\tau + \zeta_m) = \ell_p \frac{z_m}{\ell_e}. \tag{20}$$

However, since the first row is closer, it obtains larger disparities at the same screen position. As a result, displaying the k angular images at the shifts of the first row requires wider pixels. Considering

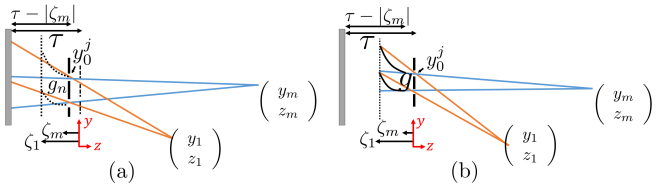

Figure 21: *Vertical resolution limits: (a) The naive pinhole solution display (dashed lines denote the equivalent z position of the vertical and horizontal barriers in our display), compared to (b) our proposed display. In our display the bound on the y resolution is set such that rays from different rows do not intersect before the slanted barriers, but can intersect between these barriers and the screen. In contrast, in the pinhole arrangement, rays from different rows cannot intersect all the way to the screen. The difference results from the fact that the screen content is different for different viewer rows in the pinhole solution, while it is identical in our solution.*

the similar triangles in Fig. 20, we can express these wider pixels as $\tilde{\ell_p}$,

$$\tilde{\ell_p} = \frac{\ell_e}{z_1}(\tau + \zeta_m). \tag{21}$$

Combining Eqs. (20) and (21) leads to

$$\tilde{\ell_p} = \frac{z_m}{z_1}\ell_p. \tag{22}$$

Thus, the number of horizontal pixels that the pinhole construction can present to the first row is in practice

$$\frac{N_x}{k\tilde{\ell_p}} = \frac{N_x}{k\ell_p} \cdot \frac{z_1}{z_m} = n_x \cdot \frac{z_1}{z_m} \tag{23}$$

■

Vertical resolution

The vertical resolution of our display is determined by g, the spacing between two adjacent slits in the vertical barrier, as calculated in Eq. (3). Similarly, let us denote by g_n the spacing between two adjacent pinhole rows. The minimal spacing g_n can be computed using arguments similar to the proof of Claim 2, and is equal to

$$g_n \geq [\frac{{y_o}^j - y_1}{z_1} - \frac{{y_o}^j - y_m}{z_m}] \cdot \frac{(\tau + \zeta_m) \cdot z_1}{z_1 + \tau + \zeta_m}. \tag{24}$$

To understand the intuition, consider Fig. 21. In our display, the vertical spacing is derived from the constraint that rays from the extreme viewer rows (row 1 and row m) should not cross each other before the end of the slanted barrier. However, it is fine for these rays to cross between the barrier and the screen, since the screen content is identical for all viewer rows. In contrast, in the pinhole solution, we must limit the vertical spacing of pinholes such that rays from different rows will not cross all the way up to the screen itself, since different viewer rows should see different pixel rows on the screen (see Fig. 10). Since the distance between the vertical barrier and the horizontal one is smaller than the distance to the screen, g is smaller than g_n. For example, with the cinema parameters described in the beginning of Sec. 5, $g = 28mm$ and $g_n = 67mm$. See also the visual comparison in Fig. 9. Note that $g = 28mm$ is the spacing obtained with our basic two-barriers solution, without angle reduction elements, but their addition can improve resolution much further.

Appendix D

Here we explain how to derive the exact shape of the slanted mirrors in our horizontal barriers (Fig. 5f). Recall that our goal is to replace

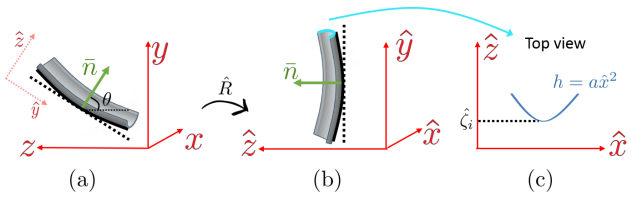

Figure 22: *The slanted mirror surface in (a) the standard coordinate system, and (b) the converted one. In (c) we demonstrate the parabola structure, i.e. a 2D slice of the surface in (b).*

the opaque surface of the slanted barrier with a reflective surface that focuses the horizontal component of the rays on the screen. As was analyzed previously, the original slanted barrier surface is defined in Claim 1 by the set of points $(\rho_i, \zeta_i), i = 1 \dots m$, and is constant along the x direction. The slanted mirror's surface, on the other hand, should focus light rays intersecting at different x coordinates; thus, it should have a parabolic structure in the x direction.

To express the surface we define a new coordinate system illustrated in Fig. 22, in which $\hat{y}$ is the direction of the best linear approximation to the slanted barrier surface and $\hat{z} = \bar{n}$ is the mean normal direction. Denoting by θ the angle between the mean normal $\bar{n}$ and the z axis, the basis conversion is given by

$$\begin{pmatrix} \hat{x} \\ \hat{y} \\ \hat{z} \end{pmatrix} = \hat{R} \begin{pmatrix} x \\ y \\ z \end{pmatrix} \tag{25}$$

with

$$\hat{R} = \begin{bmatrix} 1 & 0 & 0 \\ 0 & -1 & \tan(\theta) \\ 0 & \tan(\theta) & 1 \end{bmatrix} = \begin{bmatrix} 1 & 0 & 0 \\ 0 & & \\ 0 & & \hat{r} \end{bmatrix}. \tag{26}$$

The slanted mirror surface is composed of concave parabolic mirrors in the direction of the mean normal, and can be written as:

$$h(\hat{x}, \hat{y}) = a(\hat{y})\hat{x}^2 + \hat{\zeta}(\hat{y}), \tag{27}$$

where $a(\hat{y})$ is the parabola power and $\zeta(\hat{y})$ is the continuous function of the slanted barrier yz cross-section after the coordinate conversion. We define $\zeta(\hat{y})$ and $a(\hat{y})$ below.

To define $\zeta(\hat{y})$, note that in Claim 1 we define the cross-section of the slanted barriers as the interpolation of points $(\rho_i, \zeta_i),\ i = 1, ..., m$. These points are essentially the desired y, z coordinates of the barrier for each row of viewers (note that the spacing is uniform as a function of the viewing row, but results in a non-linear spacing along the slanted barrier curve). To define the slanted barrier in the new coordinate system $\hat{y}, \hat{z}$ we simply rotate the keypoints using

$$\begin{bmatrix} \hat{\rho}_i \\ \hat{\zeta}_i \end{bmatrix} = \hat{r} \begin{bmatrix} \rho_i \\ \zeta_i \end{bmatrix}. \tag{28}$$

We will denote these points as $\hat{\zeta}_i(\hat{y}_i)$ where $\hat{y}_i = \hat{\rho}_i$ and interpolate between them to get the continuous function $\hat{\zeta}(\hat{y})$.

We will now explain how to calculate the parabola power $a(\hat{y})$ based on Fig. 23. For a parabolic mirror to focus light at a distance f from the plane perpendicular to its normal, it should have a power of $a = -\frac{1}{4f}$. However, we want the light to focus at a distance $\tau - |\zeta_i|$ from the screen, where $\tau - |\zeta_i|$ is the distance along the (original) z axis, rather than along the normal direction $\bar{n}$. To convert the desired focusing point into a parabola power, we need to find a

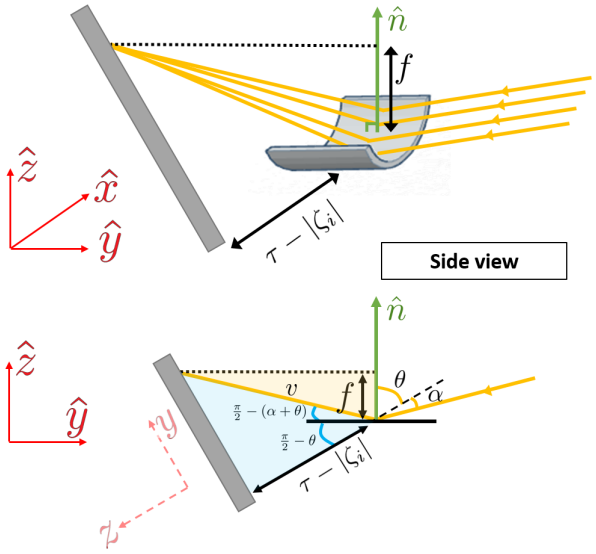

Figure 23: *Designing the focal power of the slanted horizontal mirror in order to focus rays on the screen.*

focusing distance f such that a plane at distance f from the slanted barrier (that is a plane shifted by a distance f along the direction $\bar{n}$) intersects the screen at the required point.

Let us denote the vertical angle of rays reaching the slanted barrier as $\alpha(\hat{y})$, and recall that the surface average normal direction is θ. From the geometrical relationship applied to the yellow and blue triangles in Fig. 23, we can get to the relation between $f(\hat{y})$ and the distance from the screen $\tau - |\zeta_i|$:

From the yellow triangle:

$$f = \cos(\alpha(\hat{y}) + \theta) \cdot v. \tag{29}$$

From the blue triangle:

$$v = \frac{(\tau - |\zeta_i|)}{\cos(\pi - (\alpha(\hat{y}) + 2\theta))}. \tag{30}$$

From Eqs. (29) and (30), it can be seen that if we want the rays to focus at a distance $\tau - |\zeta_i|$ from the screen, then $f(\hat{y})$, the focus distance in the normal direction, should be:

$$f(\hat{y}) = \frac{(\tau - |\zeta_i|)\cos(\alpha(\hat{y}) + \theta)}{\cos(\alpha(\hat{y}) + 2\theta)}. \tag{31}$$

The above formula gives a good approximation for the surface, but it is not accurate, since for the simplicity of the parameterization we use the mean normal direction $\bar{n}$ rather than the exact normal at each point on the slanted surface. Therefore, we perform a non-linear optimization to try to find more accurate $a(\hat{y})$ values. To implement the optimization, we use a ray-tracing function whose output is the distance between the intersection of each ray and the intended focusing point on the screen, as a function of the parabola powers $a(\hat{y})$. We use this function within Matlab non-linear optimization function fminunc, seeking values of $a(\hat{y})$ that will reduce the focusing error.

Appendix E

Table 2 provides the transitions grade (TG) evaluated on our proposed display vs. the simple lenticular sheet display.

Table 2: *Transitions Grade (TG) measures for the proposed display vs. a simple lenticular sheet display*

	angular position 1	angular position 2	angular position 3	angular position 4	angular position 5	angular position 6	angular position 7	angular position 8	angular position 9
Extreme seat - our display									
row 1	38.52	18.97	7.81	2.45	**0.53**	**0.33**	**1.51**	**5.02**	**22.06**
row 2	41.66	14.87	**5.42**	**1.56**	**0.31**	**0.40**	**1.64**	**5.71**	25.59
row 3	42.19	12.80	**4.70**	**1.45**	**0.40**	**0.51**	**1.79**	**6.00**	27.24
row 4	40.52	12.19	**4.65**	**1.65**	**0.58**	**0.63**	**1.96**	**6.53**	27.96
row 5	38.73	12.18	**4.92**	**2.00**	**0.83**	**0.82**	**2.15**	**7.01**	28.14
row 6	37.23	13.05	**5.59**	**2.48**	**1.14**	**0.95**	**2.21**	**7.00**	26.98
row 7	35.72	13.38	**6.09**	**2.93**	**1.45**	**1.14**	**2.40**	**7.26**	26.16
row 8	34.66	13.81	**6.78**	**3.43**	**1.76**	**1.35**	**2.53**	**7.27**	24.94
row 9	33.79	13.99	**7.39**	**3.88**	**2.11**	**1.56**	**2.64**	**7.27**	24.11
row 10	32.94	14.31	**8.04**	**4.45**	**2.46**	**1.75**	**2.67**	**7.09**	23.19
Extreme seat - lenticular sheet display									
row 1	**26.20**	**5.91**	**2.07**	**0.60**	**0.24**	1.01	2.64	6.55	23.66
row 2	**10.54**	**9.90**	9.18	8.68	8.32	8.03	7.73	7.38	**8.72**
row 3	**9.18**	**9.22**	9.22	9.15	8.79	8.41	8.07	7.82	**9.35**
row 4	**8.99**	**9.00**	9.00	8.97	8.85	8.55	8.28	8.71	**9.21**
row 5	**9.08**	**9.06**	9.04	8.81	8.59	8.35	8.24	8.96	**9.03**
row 6	**8.91**	**8.63**	8.43	8.31	8.27	8.26	8.74	9.23	**9.26**
row 7	**8.65**	**8.68**	8.70	8.67	8.63	8.73	9.35	9.50	**9.39**
row 8	**9.00**	**8.88**	8.62	8.47	8.25	8.55	9.03	9.00	**9.05**
row 9	**8.65**	**8.67**	8.65	8.61	8.76	9.25	9.35	9.31	**9.38**
row 10	**8.58**	**8.40**	8.34	8.35	8.67	9.05	9.04	9.06	**9.07**
Middle seat - our display									
row1	36.55	9.29	2.60	0.57	0.12	0.34	1.83	7.49	35.28
row 2	40.69	**6.47**	**1.37**	**0.18**	**0.01**	**0.08**	**0.89**	**5.20**	39.28
row 3	42.56	**5.02**	**0.85**	**0.06**	**0.00**	**0.02**	**0.49**	**4.13**	41.24
row 4	43.25	**4.51**	**0.63**	**0.03**	**0.00**	**0.00**	**0.33**	**3.81**	42.13
row 5	43.47	**4.49**	**0.57**	**0.02**	**0.00**	**0.00**	**0.26**	**4.01**	42.52
row 6	42.92	**4.90**	**0.62**	**0.04**	**0.00**	**0.00**	**0.29**	**4.40**	41.96
row 7	42.35	**5.47**	**0.67**	**0.05**	**0.00**	**0.01**	**0.34**	**4.84**	41.26
row 8	41.61	**6.11**	**0.78**	**0.08**	**0.00**	**0.01**	**0.43**	**5.38**	40.74
row 9	41.12	**6.58**	**0.97**	**0.10**	**0.00**	**0.02**	**0.54**	**5.86**	39.89
row 10	40.45	**7.16**	**1.19**	**0.14**	**0.01**	**0.03**	**0.67**	**6.25**	39.41
Middle seat - lenticular sheet display									
row 1	**24.49**	**0.29**	**0.00**	**0.00**	**0.00**	**0.00**	**0.00**	**0.95**	**30.55**
row 2	**6.84**	7.94	9.70	10.26	10.37	10.36	10.22	9.03	**7.63**
row 3	**9.15**	9.11	9.05	8.96	8.41	8.00	8.71	8.97	**9.06**
row 4	**8.77**	8.83	8.90	8.92	8.95	8.98	8.96	8.96	**8.92**
row 5	**9.07**	9.05	9.02	9.01	8.96	8.48	8.02	8.68	**9.00**
row 6	**8.29**	8.34	8.95	9.23	9.23	9.25	9.25	9.24	**9.24**
row 7	**9.45**	9.19	8.72	8.65	8.62	8.62	8.68	8.69	**8.66**
row 8	**9.03**	9.05	8.98	9.02	9.04	8.92	8.62	8.22	**8.27**
row 9	**8.64**	8.63	8.67	8.63	8.66	9.12	9.36	9.33	**9.39**
row 10	**8.36**	8.71	9.02	9.05	9.05	9.06	9.05	9.06	**9.06**